Supporting Information

Highly selective NIR probe for intestinal *β*-Glucuronidase and High-throughput screening inhibitors to therapy intestinal damage

Lei Feng,[†,§,#] YongLiang Yang,[§,#] Xiaokui Huo,[†,#] Xiangge Tian,[†,#] Yujie Feng,[†] Hanwen Yuan,[‡] Lijian Zhao,[⊥] Chao Wang,[†,§,*] Peng Chu,[§] Feida Long,[§] Wei Wang,[‡,*] Xiaochi Ma[†,*]

[†] College of Integrative Medicine, College of Pharmacy, the National & Local Joint Engineering Research Center for Drug Development of Neurodegenerative Disease, Dalian Medical University, Dalian 116044, China

[‡] TCM and Ethnomedicine Innovation & Development International Laboratory, Sino-Pakistan TCM and Ethnomedicine Research Center, School of Pharmacy, Hunan University of Chinese Medicine, Changsha 410208, China

[§]Center for Molecular Medicine, School of Life Science and Biotechnology, State Key Laboratory of Fine Chemicals, Dalian University of Technology, Dalian 116024, China

[⊥]Bio/Medical Experiment Center, College of Biology, Hunan University, Changsha, 410082, China

Corresponding Author

*E-mail: wach_edu@sina.com (C. Wang)
*E-mail: wangwei402@hotmail.com (Wei Wang).
*E-mail: maxc1978@163.com (X. C. Ma)

Author Contributions

[#] L. Feng, Y. Yang, H. Huo and X. Tian contributed equally to this work.

Index

Experimental Section

Materials and instruments.

Lysozyme, N-acetyl glucosaminidase (NAG), Carbonic anhydrase (Cas), Proteinase K (Pak), Carboxylesterases (CE1b, CE1c, CE2), *β*-Galactosidase (*β*-Gla), *β*-Glucosidase (*β*-Glc), *α*-Glucosidase (*α*-GLC), GLU (*Escherichia coli*) were all obtained from Sigma-Aldrich. Bovine serum albumin (BSA), Glutamate, Glutamine, Glycine, Serine, Glutathione, Arginine, lysine, Cysteine, Tryptophan, Glucose, Tyrosine, Bilirubin, and Myristic acid were purchased from Shanghai yuanye (Shanghai, China). Bis-pnitrophenyl phosphate (BNPP), loperamide (LPA), α-galactose and baicalin were purchased from J&K Chemicals. All fluorescence tests performed on Synergy neo Microplate Reader (Bio-Tek). Constant temperature incubator shaker (ZHWY-2012C) was the production of Shanghai Zhicheng Analytical Instrument Co. Ltd (P.R. China). The confocal fluorescence images of bacteria were required using Leica Confocal Microscope with the excited wavelength λ_{ex} 633 nm and emission filter of λ_{em} 645 – 690 nm (Leica, German). The imaging of mice and gut were recorded in a NightOWL II LB983 small animal *in vivo* imaging system equipped with a sensitive Charge Coupled Device (CCD) camera, with an excitation laser of 630 nm and an emission filter of 665 – 735 nm. The fluorescence images of bacterial colonies on plates were obtained using PerkinElmer Invivo system with λ_{ex} 605 nm/λ_{em} 660 nm.

NMR spectra were required using a Bruker 501. Accurate mass detection was measured on fourier transform ion cyclotron resonance mass spectrometer (LTQ Orbitrap XL). The hydrolysis supernatants were determined by HPLC-UV analysis (Waters e2695 equipped with 2998 PDA Detector). All other reagents and solvents

used were of the highest grade commercially available. *Enterobacter cloacae*, *Escherichia coli*, *Escherichia coli* ETEC, *Escherichia coli* EPEC, *Escherichia coli* EAEC, *Enterococcus faecalis*, *Klebsiella oxytoca*, *Klebsiella Pneumoniae*, *Monilia albican*, *Pseudomonas Aeruginosa*, *Staphyloccocus aureus* Rosenbach, and *Streptococcus agalactiae* were purchase from China General Microbiological Culture Collection Center.

Synthesis and characterization of DDAO-glu.

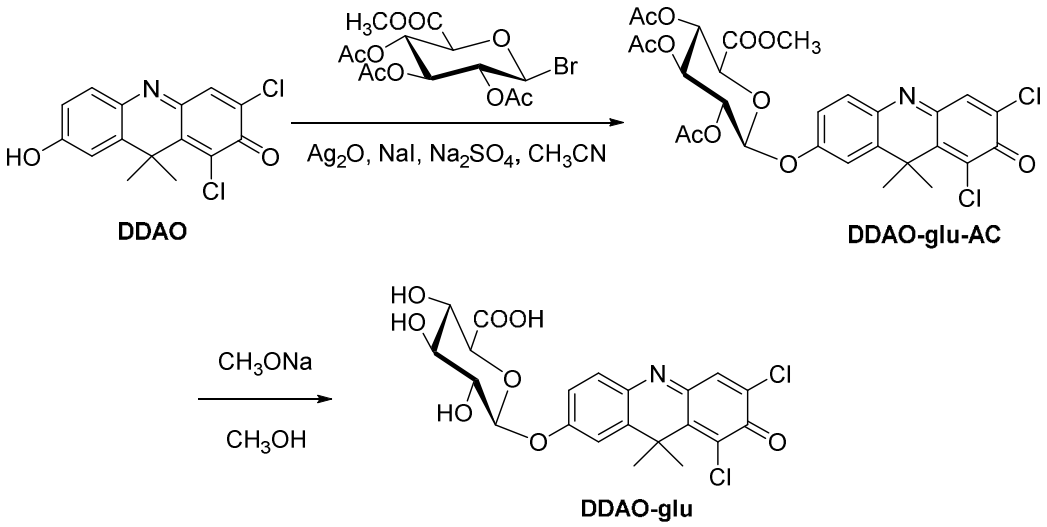

Figure S1. The synthesis pathway of **DDAO-glu**.

*Synthesis of Compound **DDAO-glu-AC**.* **DDAO** (48 mg, 0.2 mmol), bromo-2,3,4-tri-O-acetyl-α-D- glucopyranuronic acid methyl ester (400 mg, 1 mmol), Ag_2O (463 mg, 2 mmol), NaI (150 mg, 1 mmol) and a sufficient amount of anhydrous Na_2SO_4 were dissolved in dry CH_3CN (10 mL) in a 25 mL round bottom flask and stirred at room temperature under a nitrogen atmosphere for 48 h, filtered, and evaporated. The residue was purified by chromatography (silica gel, EtOAc–hexane as eluent, 1:5, v/v) to afford 50 mg **DDAO-glu-AC** as an orange solid (Yield 45.2%). ^{1}H NMR (500 MHz, $CDCl_3$) δ 7.74 (s, 1H), 7.35 (d, J = 10.1 Hz, 1H), 6.73 – 6.61 (m, 2H), 5.44 (dt, J = 14.7, 4.7 Hz, 1H), 5.35 (ddd, J = 17.8, 13.2, 8.3 Hz, 3H), 4.09 – 3.89 (m, 1H), 3.70 (s, 3H), 2.11 (s, 3H), 2.06 (s, 3H), 2.03 (s, 3H), 1.78 (d, J = 5.6 Hz, 6H). ^{13}C NMR (125 MHz, $CDCl_3$) δ 187.27, 170.12, 169.38, 169.24, 166.53, 153.19, 149.45, 148.29, 140.85, 140.81, 133.27, 132.65, 132.36, 130.41, 128.87, 128.25,

100.68, 72.66, 71.91, 71.34, 69.19, 52.84, 38.09, 28.80, 28.76, 20.73, 20.61, 20.47. HRMS (ESI positive) calcd. for $C_{28}H_{27}Cl_2NNaO_{11}^+$ $[M+Na]^+$ 646.0853, found 646.0853.

*Synthesis of Compound **DDAO-glu**.* **DDAO-glu-AC** (28 mg, 0.05 mmol) was dissolved in 10 mL of MeOH, and MeONa (108 mg, 2 mmol) was added, the mixture was stirred at room temperature for 3 h, then evaporated, and the resulting residue was purified by HPLC (a linear gradient formed from 0.03% trifluoroacetic acid (TFA) water (A) and acetonitrile (B): 0.0 – 5.0 min, 15% B, 5.0 – 25.0 min, 20% - 90% B, 25.0 – 30.0 min, 90% B. The flow rate was set at 2 mL/min) to afford 9 mg. **DDAO-glu** as a light yellow solid (Yield 43.6%).^{1}H NMR (500 MHz, CD_3OD) δ_H 7.69 (s, 1H), 7.60 (d, J = 8.7 Hz, 1H), 7.35 (d, J = 2.3 Hz, 1H), 7.17 (dd, J = 8.7, 2.3 Hz, 1H), 5.14 – 5.01 (m, 1H), 3.85 (d, J = 7.0 Hz, 1H), 3.57 – 3.53 (m, 3H), 1.90 (d, J = 1.6 Hz, 6H). ^{13}C NMR (125 MHz, CD_3OD) δ_C 174.46, 162.64, 149.27, 142.70, 141.83, 140.72, 137.82, 137.63, 135.54, 134.83, 117.36, 116.69, 101.84, 77.74, 76.55, 74.67, 73.52, 40.58, 26.96. HRMS (ESI negative) calcd. for $C_{21}H_{18}Cl_2NO_8^-$ $[M-H]^-$ 482.0415, found 482.0405.

Spectroscopic data of DH-1, -2, -3 from *Rheum palmatum* L.

(-)-epicatechin 3-gallate (DH-1). ^{1}H NMR (600 MHz, CD_3OD) δ_H 2.85 (1H, dd, J = 17.4, 2.4 Hz), 2.99 (1H, dd, J = 17.4, 4.8 Hz), 5.03 (1H, s), 5.52 (1H, m), 5.95 (1H, d, J = 2.4 Hz), 5.96 (1H, d, J = 2.4 Hz), 6.69 (1H, d, J = 8.4 Hz), 6.81 (1H, dd, J = 8.4, 1.8 Hz), 6.93 (1H, d, J = 1.8 Hz), 6.95 (2H, s). ^{13}C NMR (150 MHz, CD_3OD) δ_C 26.86, 69.97, 78.63, 95.86, 96.51, 99.36, 110.19 (× 2), 115.09, 115.98, 119.37, 121.45, 131.45, 139.78, 145.94, 145.97, 146.31, 157.21, 157.23, 157.78, 157.83, 167.59. ESI-MS m/z 443.1 $[M+H]^+$.

6-hydroxymusizin-8-*β*-D-glucopyranoside (DH-2). ^{1}H NMR (600 MHz, CD_3OD) δ_H 2.27 (3H, s), 2.58 (3H, s), 3.45-3.55 (3H, m), 3.77 (1H, dd, J = 12.0, 6.0 Hz), 3.91 (1H, dd, J = 12.0, 1.8 Hz), 3.98 (1H, dd, J = 12.0, 1.8 Hz), 5.08 (1H, d, J = 7.8 Hz), 6.69 (1H, d, J = 1.8 Hz), 6.90 (1H, brs), 6.96 (1H, d, J = 1.8 Hz). ^{13}C NMR (150 MHz, CD_3OD) δ_C 18.92, 31.20, 61.04, 69.79, 73.52, 76.75, 77.43, 102.91, 103.10, 103.98, 118.29, 133.87, 138.08, 152.67, 156.03, 156.83, 206.81. ESI-MS m/z 395.2 $[M+H]^+$.

1,2-di-O-galloyl-6-cinnamoyl-β-D-glucose (DH-3). ^{1}H NMR (600 MHz, DMSO-d_6) δ_H 3.52 (1H, t, J = 9.0 Hz), 3.71 (1H, brt, J = 9.6 Hz), 3.81 (1H, m), 4.31 (1H, brd, J = 10.8 Hz), 5.01 (1H, t, J = 9.0 Hz), 5.64 (1H, brs), 5.68 (1H, brs), 5.81 (1H, d, J = 8.4 Hz), 6.62 (1H, d, J = 16.2 Hz), 6.90 (2H, s), 6.97 (2H, s), 7.41 (3H, m), 7.68 (3H, m). ^{13}C NMR (150 MHz, DMSO-d_6) δ_C 63.25, 69.95, 73.26, 73.90, 75.26, 92.58, 108.2, 109.06 (× 2), 109.40 (× 2), 118.08, 118.16, 119.65, 121.7, 128.90 (× 2), 129.41 (× 2), 131.08, 134.29, 139.04, 139.89, 145.67, 146.02 (× 2), 146.08 (× 2), 164.67, 165.85, 166.16. ESI-MS *m/z* 615.3 $[M+H]^+$.

Kinetics study.

In order to estimate the kinetic parameters of **DDAO-glu** for GLU, the kinetics were performed in different sources of GLUs. Briefly, **DDAO-glu** (0 − 600 μM) was incubated with different sources of GLU including from *E.coli*, *E.coli*-IX-A, *E.coli*-VII-A and *E.coli*-K12 for 30 min, which ensured less than 20% of substrate was metabolized, and the formation rates of **DDAO** were in relation to incubation time and protein concentration in the linear range. The apparent K_m and V_{max} values were calculated from nonlinear regression analysis of experimental data according to biphasic equation (1).

$$v=\frac{V_{max1}\times[S]}{K_{m1}+[S]}+\frac{V_{max2}\times[S]}{K_{m2}+[S]} \quad \text{.....(1)}$$

The V_{max} represents the maximal rate and K_m is the substrate concentration at the half-maximal rate. Kinetic constants were obtained using Origin 7.5 (origin Lap Corp. Northampton. MA.USA) and produced as the mean ± SD of the parameter estimate.

Quantification of GLU in human feces.

DDAO-glu was further used to evaluate the GLU activity in human feces. Twenty-four human fecal specimens from volunteers (23–60 years; 12 men and 12 women) were collected for feces preparation according to Tamura et al. Sample (about 0.2 g) were suspended in 3-fold cold saline and mixed and homogenized (IKA-T 10 homogenizer; IKA, Staufen, Germany) for approximately 1 min in ice bath. The suspension was centrifuged at 200 g for 5min. After three freeze-thaw cycles from liquid nitrogen to room temperature, the supernatant was centrifuged at 10000 g for

20 min. The resulting supernatant was used for the assessment of GLU activity using **DDAO-glu** as described above. The catalytic activity was corrected by the amount of protein of each feces sample. Protein concentrations of feces preparations were measured by BCA assays (Solarbio, China). GLU activity was also determined using commercial kit according to the manufacturer's instructions (Nanjing Jiancheng Institute of Biotechnology, Nanjing, China). The correlation between the experimental results determined by **DDAO-glu** and commercial kit was analyzed using Pearson correlation analysis (Graphpad Software, La Jolla, California).

Intestinal distribution of GLU in mouse

In the intestinal distribution of GLU experiment, mice fasted overnight were anesthetized and the whole intestinal segments were removed and divided into seven segments: **1** duodenum (starting 1 cm below the pylorus); **2 − 6** small intestine (**2 − 4** jejunum, upper small intestine; **5** and **6** ileum, lower small intestine) and **7** colon. Each intestinal segment was flushed with cold saline and immediately placed in 37 ℃ oxygenated (O_2/CO_2, 95%:5%) buffer solution. The reaction was started by adding **DDAO-glu** (100 μM). Following 30-min incubation, the segment was washed by cold saline three times and then imaged by the small animal imaging system, with excitation at 630 nm and semiconductor laser emission collected at 665 – 735 nm.

Isolation and identification of active compounds from *Rheum palmatum* L.

The roots of Rheum palmatum (2 kg) were powdered and extracted with ethanol refluxed (10 L × 3). After the evaporation of ethanol, the extracts were separated by HPLC with a Waters Prominence HPLC system equipped with a Waters 2767 sample manager, a Waters 2545 binary Gradient Module, a Waters 2489 UV/Visible Detector and a Waters XBridge C18 (19 mm × 250 mm, 5 μm) chromatograph column. Then 1-23 fractions were obtained by a gradient elution chromatographic method. The mobile phase consisted of acetonitrile-water (10:90) (A) and acetonitrile (B), with the gradient condition (0.0 - 20.0 min, 20% B, 20.0 - 55.0 min, 20% -70% B, 55.0 - 70.0 min, 70 - 90% B, 70 - 80 min 90% B). The flow rate was set at 10 mL/min and the injection volume was 300 μL with the concentration of crude extract 50 mg/mL. The UV detection was set at 280nm. The fractions were automatically collected for those

target chromatographic peaks with the detected values ≥ $2.0\times e^{-2}$ mAU. Totally, 23 fractions of HPLC were prepared for the next high-throughput inhibition assay for GLU. With the guidance of the inhibitory effects evaluation against GLU, the fractions **6**, **11** and **13** were further purified by the preparative HPLC equipped with DAD detector, which gave the compounds **DH-1**, **DH-2**, and **DH-3** identified by the spectral data (MS and NMR).

Inhibition kinetic of the active compounds toward GLU.

After a high-throughput screening and further isolation under the guidance of activity tracking, three target compounds from *R. palmatum L.* which significantly inhibited the activity of GLU were identified and evaluated. Next, the inhibition activity of **DH-1**, **-2**, and **-3** toward GLU were performed and their inhibitory IC_{50} values toward GLU were also determined, respectively. Furthermore, in order to illustrate the mechanism of this inhibition phenomenon, the inhibition kinetic of **DH-1** was performed. Briefly, after the above inhibitory IC_{50} value of **DH-1** was determined, next, different concentrations of **DDAO-glu** was added in our standard incubation system in the presence a range concentrations of **DH-1**. Finally, the Dixon plots and Lineweaver–Burk plots were described by fitting the above data. Following the inhibition kinetic type was determined by the intersection point in the Dixon and Lineweaver–Burk plots.

Computational modeling and molecular dynamics (MD) simulation.

The crystallographic structure of GLU was obtained from the Protein Data Bank (PDB) database (PDB code: 3LPF). The crystallographic structure of hβG (PDB code: 3HN3) was used as a template to build the tetramer structure of GLU which was used for all the simulation. Molecular docking was performed using our newly developed in-house docking tool FIPSDock. The ligand and protein input structures in the simulations were saved using PDBQT file format. All of the MD simulations were performed by Gromacs 4.6.7 with Amber99sb force field. The general amber force field (GAFF) parameters for DH-1 were built by UCSF Chimera and ACPYPE with AM1-BCC charges. The protocol of the MD simulation was as follows as described previously: 1) The complex structure was solvated in a truncated octahedron TIP3P

water box with 1 nm distance from the edge and relaxed using 1000 steps of steep descent minimization followed by 5000 steps of conjugate gradient minimization; 2) the complex was then equilibrated under standard NVT conditions for 1 ns; 3) after the equilibration run, a 5 ns simulation at constant pressure with a target temperature of 300 K and pressure of 1 atm was conducted. Particle mesh Ewald (PME) method implemented in Gromacs 4.6.7 was used to treat the long-range electrostatic interactions in the production phase. The LINCS algorithm was employed to restrain the hydrogen positions at their equilibrium distances; 4) both energies and coordinates were saved every 10 ps for the postproduction analysis. After 5 ns MD simulation, the molecular mechanics energies combined with the Poisson–Boltzmann surface area continuum solvation (MM/PBSA) methods were employed to estimate the free energy of the binding of **DH-1** with GLU tetramer structure. The Ligplot program version 4.53 was used to generate the interaction map between **DH-1** with GLU tetramer active site. Pymol educational version was used to generate all the other figures.

High-throughput screening of GLU inhibitor from herbal medicines by using DDAO-glu.

Nowadays, herbal medicines were widely and safely used in our daily life. In order to investigate the inhibition effect of herbal drugs toward GLU, a high-throughput screening was developed by using our probe **DDAO-glu**. Firstly, the extraction and preparation of herbal medicines were performed as follows: each sample (5 g of dried plant sample) was accurately weighted and ground to fine particles, and then passed through a 40-mesh screen. Plant materials were extracted with 95% ethanol (100 mL) by ultrasonication at room temperature for 60 min after cooling extraction for 12 h. The extraction process was repeated for three times, and the extracts were filtered and then collected *in vacuo*. The crude extract was dissolved in methanol (4 mg/mL), and then followed by centrifugation at 10000 rpm for 10 min at 4 °C. And then, dried extract was dissolved in DMSO for 2 mg/mL as a stock solution, these extracts of 50 herbal medicines was added in our standard system in the presence of **DDAO-glu** (10 μM) at the finial concentration of 10 μg/mL (containing less than 1% DMSO). The same control volume of DMSO instead of herbal extract as control groups in the same

incubation system. At last, after incubation at 37 °C for 30 min, 100 μL ice-cold acetonitrile was added to terminate the reaction then 200 μL reaction solution was transferred into a 96-well plates following a imaging in a NightOWL II LB983 small animal *in vivo* imaging system containing a sensitive Charge Coupled Device (CCD) camera, with an excitation laser of 630 nm and an emission filter of 665 - 735 nm. Comparing with the group, the residual activity was analyzed in the software Bruker MI SE by semi-quantitative of the fluorescence imaging.

Effects of ECG on diclofenac pharmacokinetics and diclofenac-induced intestine damage following oral administration.

Effect of **ECG** on diclofenac pharmacokinetics was assessed in rats. After fasting overnight (12 h, free access to water), rats received a single dose of diclofenac (10 mg/kg) alone or combined with **ECG** (50 mg/kg) suspended in water from a gavage needle. Blood samples were drawn from the back jugular vein (jugular vein intubation operation performed the day before) into heparinized 1.5 mL polythene tubes at 0, 1, 5, 15, 30, 60, 90, 120, 180, 240, 300, 360, 420, 480, and 600 min after oral administration of diclofenac. The samples were immediately centrifuged to obtain plasma. After deproteinization by acetonitrile and centrifugation at 16,099 g for 10 min, plasma concentration of diclofenac was determined using LC-MS/MS (Shimadzu LC system, Chiyoda-Ku, Kyoto, Japan. AB SciexQTrap® 4500 mass spectrometer, Applied Biosystems, Concord, Ontario, Canada.). Diclofenac was determined by multiple reactions monitoring (MRM) operated in the negative electrospray ionization (ESI) mode with the selected *m/z* transition of 294.0 → 248.9.

Rat intestinal injury was investigated after oral administration of diclofenac with or without ECG. Rats were divided randomly into three groups: (1) diclofenac (10 mg/kg) group, (2) diclofenac (10 mg/kg) + **ECG** (50 mg/kg) group, (3) control group. Rats in diclofenac group and diclofenac + **ECG** group received oral administration of diclofenac (10 mg/kg) alone or combined with **ECG** (50 mg/kg) suspended in water from a gavage needle for 6 days, respectively. Rats in control group received an equivalent volume of water. On two hours after the last administration, all animals were euthanized and the ileum were harvested for fluorescence detection as described

above and for further evaluation of diclofenac-induced enteropathy by nitroblue tetrazolium (NBT) staining as previously described. In brief, the intestine was opened longitudinally along the antimesenteric side and rinsed in ice-cold PBS. Then, the tissue were incubated for 15 min in 1 mM NBT solution containing 16 mM HEPES, 125 mM NaCl, 3.5 mM KCl, and 10 mM glucose. Next, the tissues were fixed in 10% formalin for 24 h and transferred to 70% ethanol. The luminal side of the intestine was photographed with a LUMINESCENT IMAGE ANALYZER (Amersham Imager 600, GE Healthcare Bio-Sciences AB, Uppsala, Sweden). Representative parts of the formalin-fixed tissues were embedded in paraffin, processed by standard histological techniques, stained with haematoxylin and eosin (H&E), and examined for morphological evidence of intestinal injury. Another fresh intestinal tissues (about 100 mg each) were sliced and homogenized (IKA-T 10 homogenizer; IKA, Staufen, Germany) in 0.9 mL cold saline. After centrifuged at 1000 g for 10 min, the supernatant was used for determining the levels of ATP, LDH, GSH, MDA, MPO, Caspase-3, and Caspase-9 by commercial kits according to the manufacturer's manual (Nanjing Jiancheng Institute of Biotechnology, Nanjing, China).

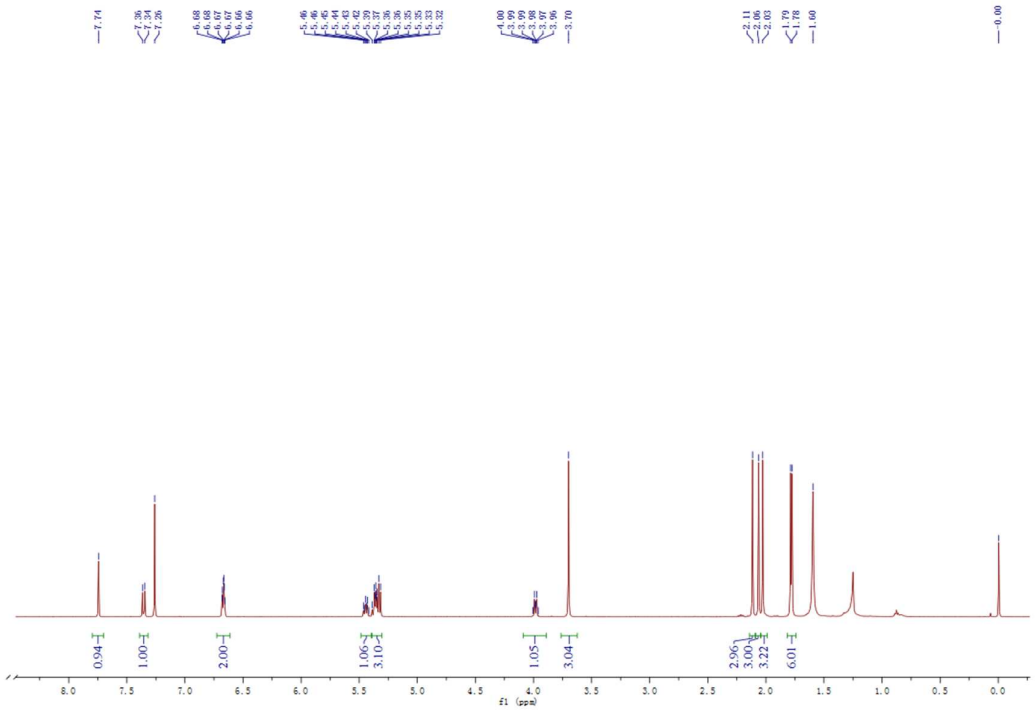

Figure S2. ^{1}HNMR spectrum of **DDAO-glu-AC** (500 MHz, $CDCl_3$)

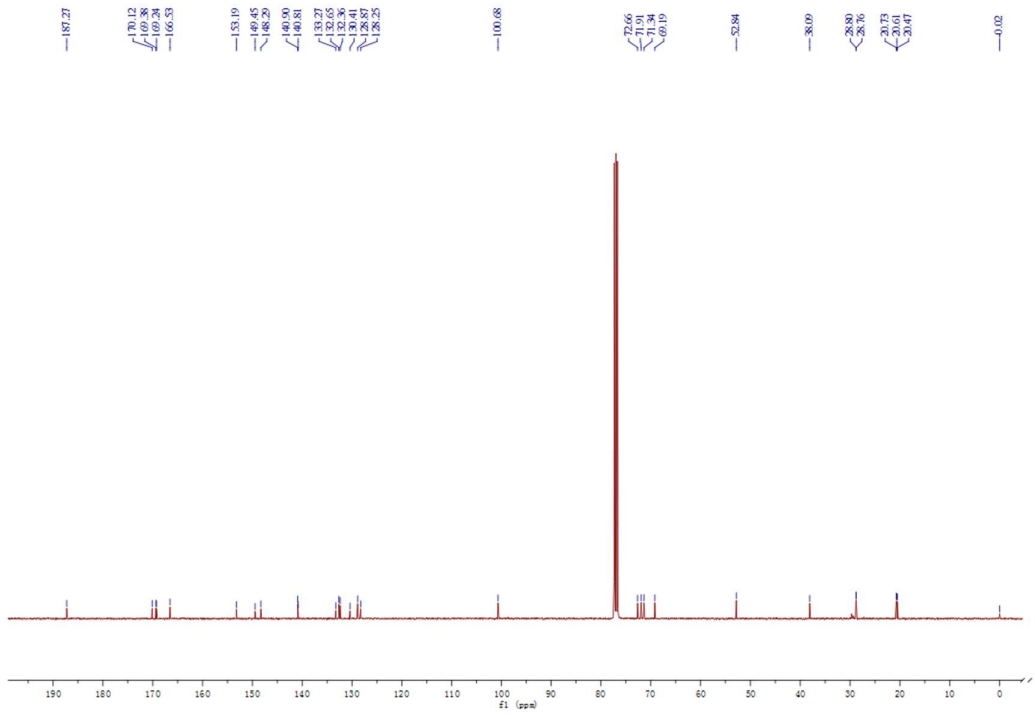

Figure S3. ^{13}C NMR spectrum of **DDAO-glu-AC** (125 MHz, $CDCl_3$)

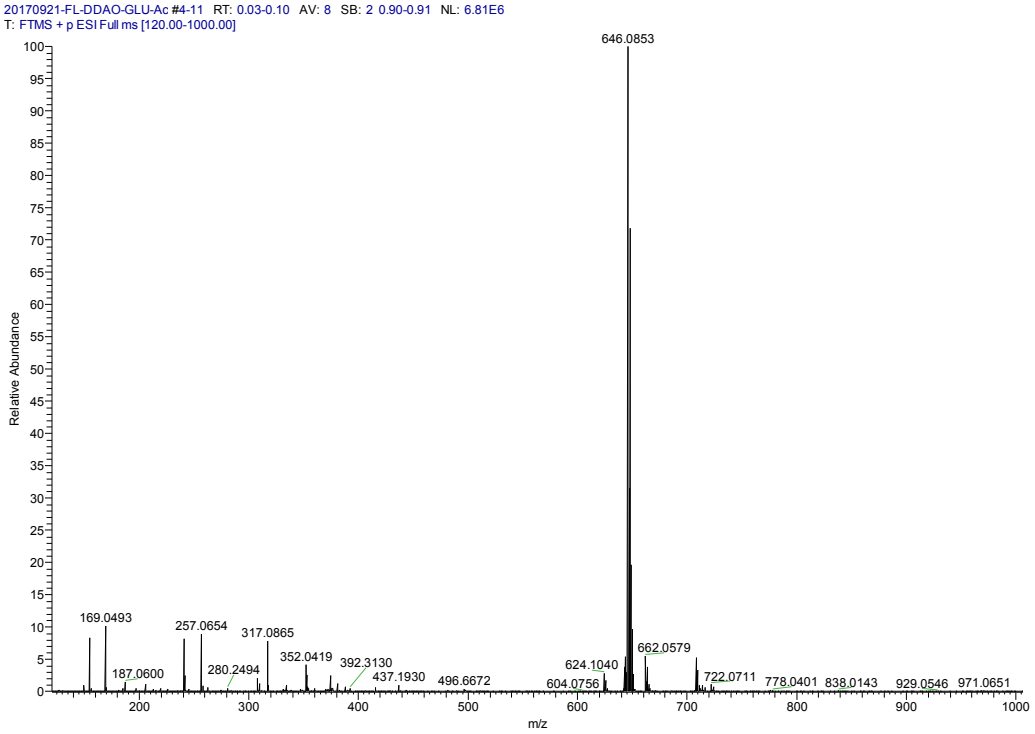

Figure S4. HRMS of **DDAO-glu-AC**

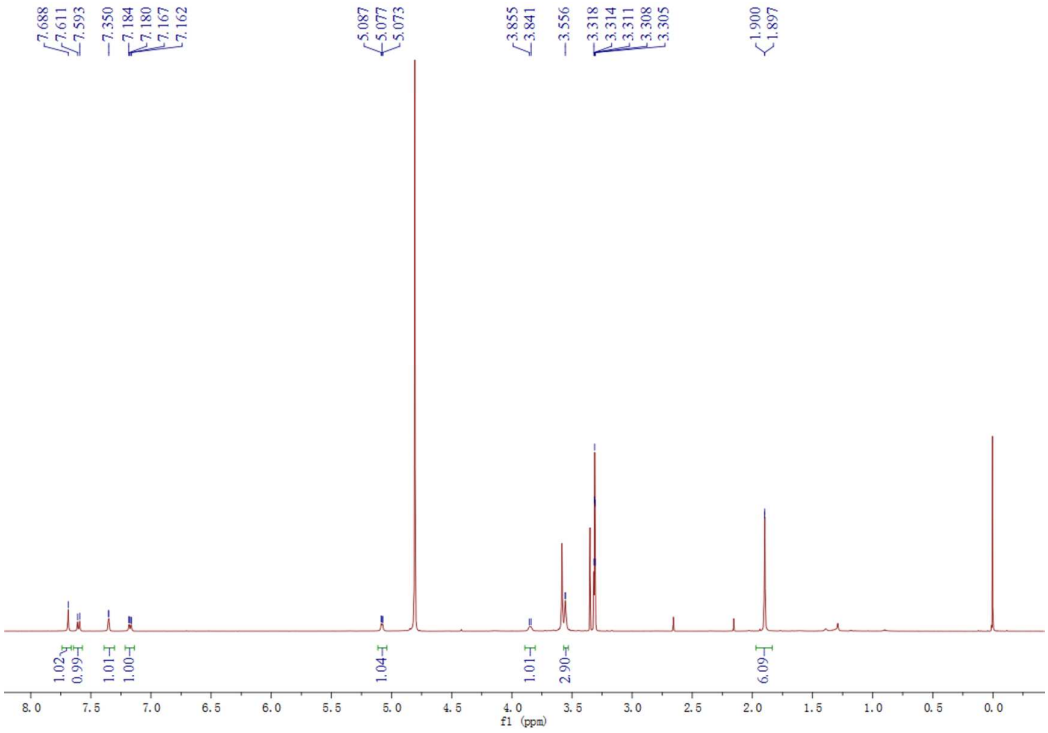

Figure S5. [1]HNMR spectrum of **DDAO-glu** (500 MHz, CD_3OD)

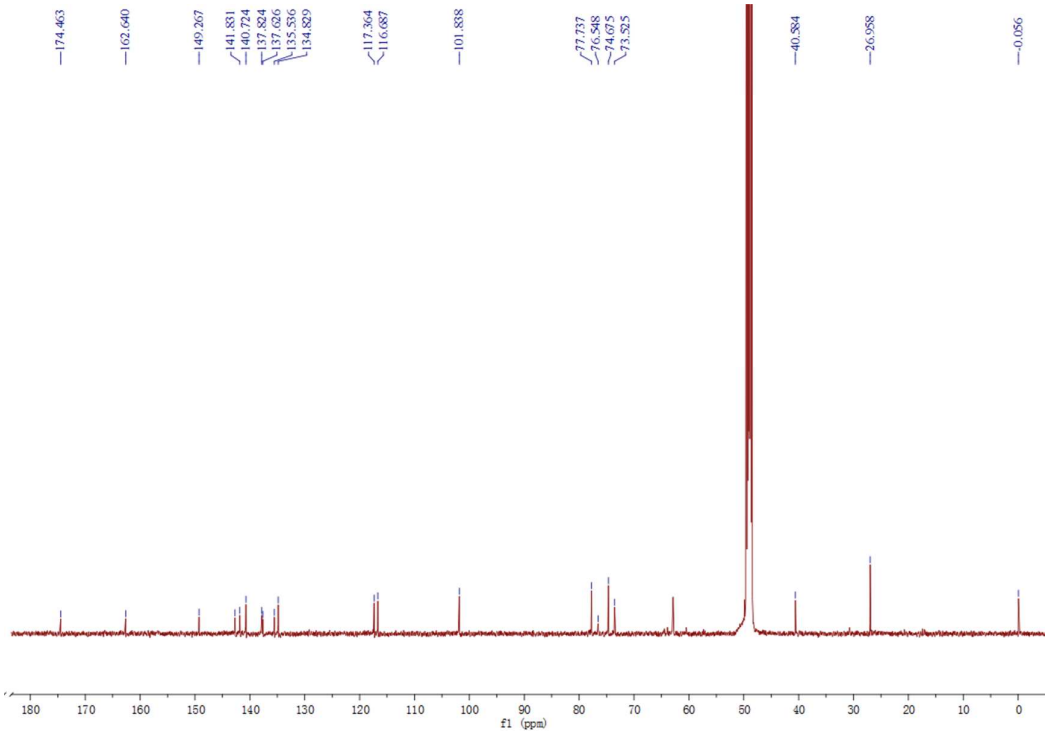

Figure S6. ^{13}C NMR spectrum of **DDAO-glu** (125 MHz, CD_3OD)

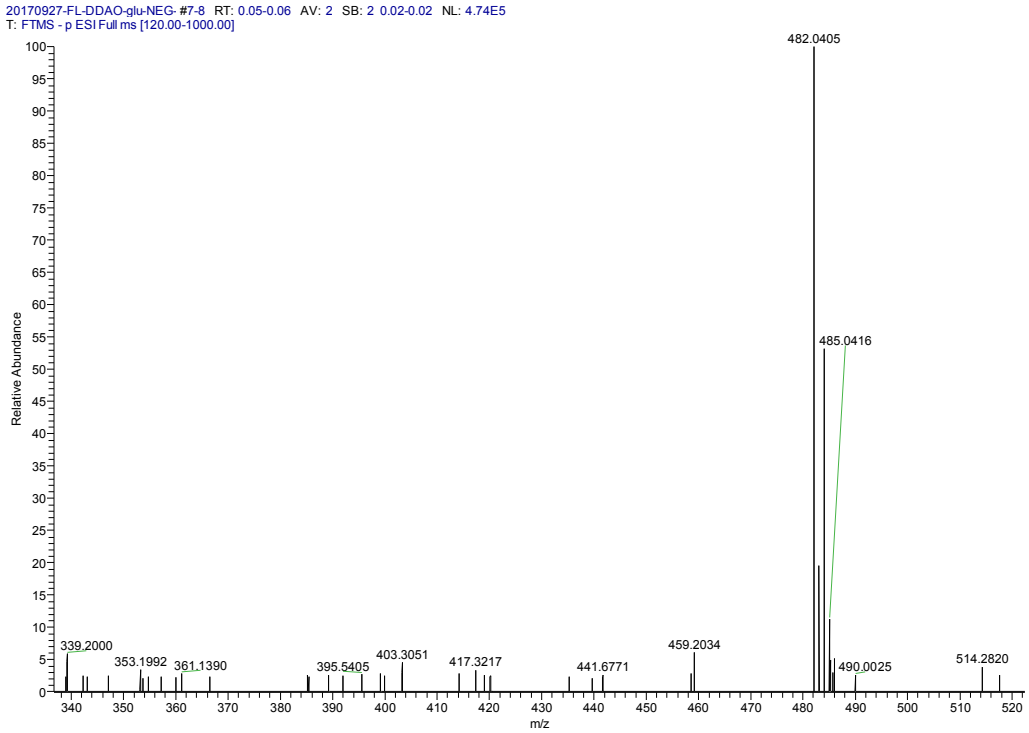

Figure S7. HRMS of **DDAO-glu.**

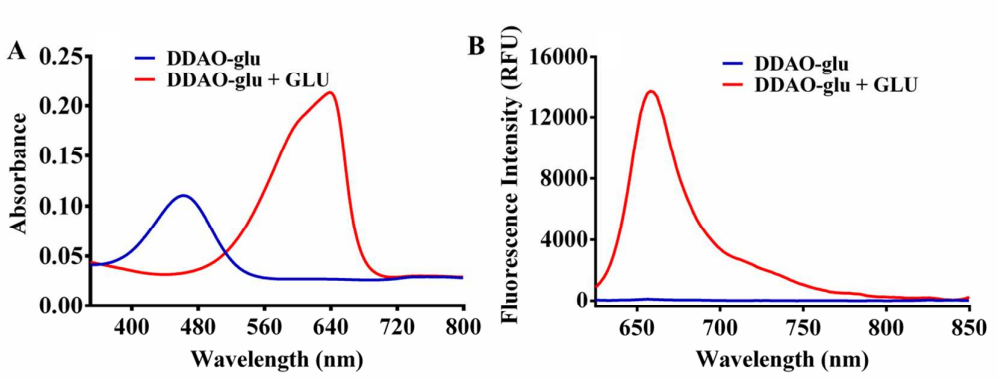

Figure S8. Absorption (A) and fluorescence emission (B) spectra of **DDAO-glu** before (blue) and after (red) incubating with GLU at 37 °C for 30 min in PBS buffer (pH = 7.0).

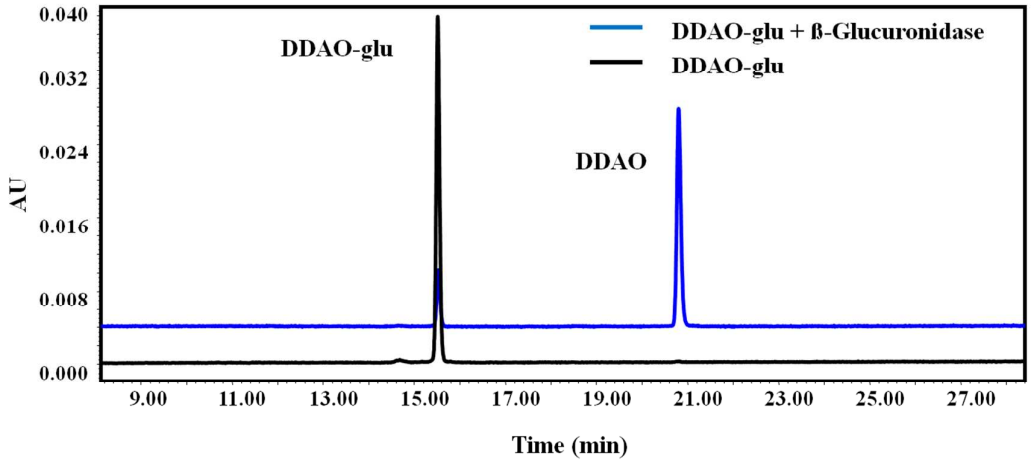

Figure S9. Representative HPLC chromatograms of **DDAO-glu** (10 μM) incubation samples at 37 ºC, UV detector was set at 484 nm.

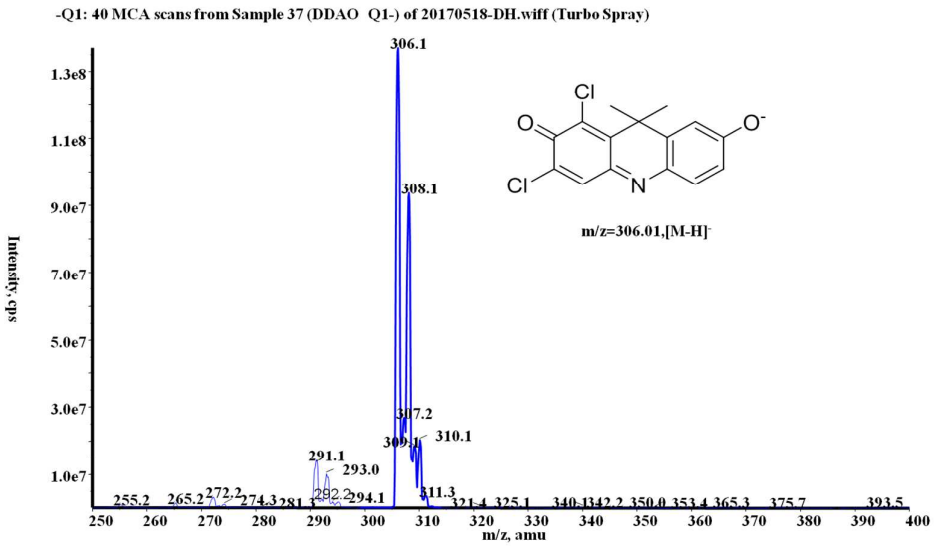

Figure S10. LC/MS spectrum of the metabolite of **DDAO-glu.**

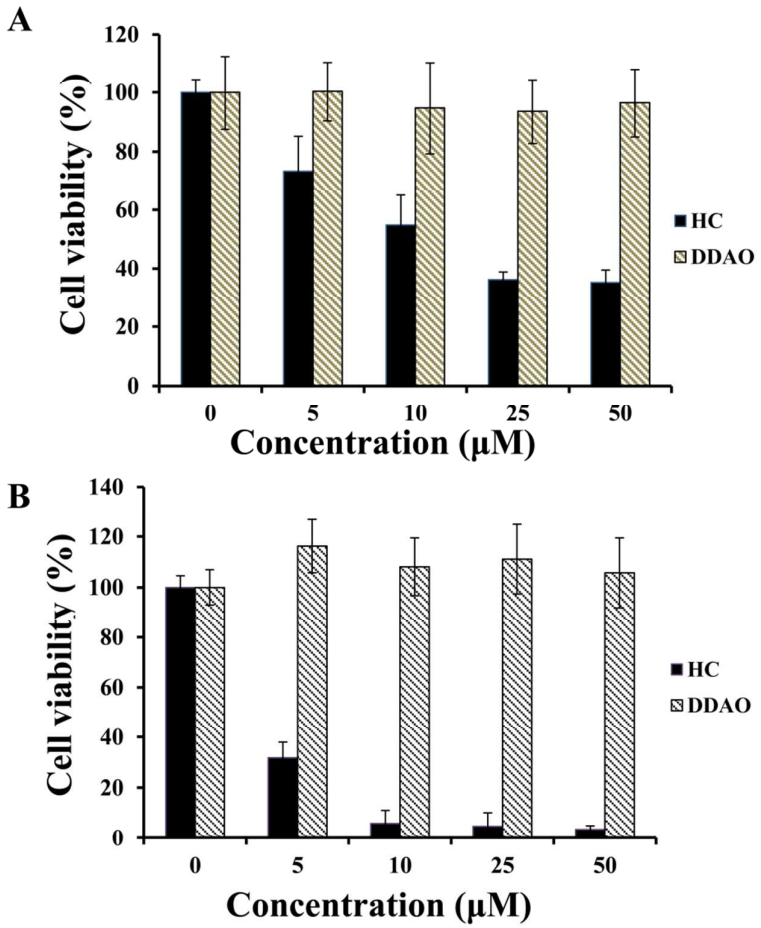

Figure S11. Cytotoxicity of **DDAO** and **HC** on Human Umbilical Vein Endothelial Cells (**HUVEC**, **A**), and human liver hepatocellular carcinoma cells (**HepG2**, **B**) at different concentrations.

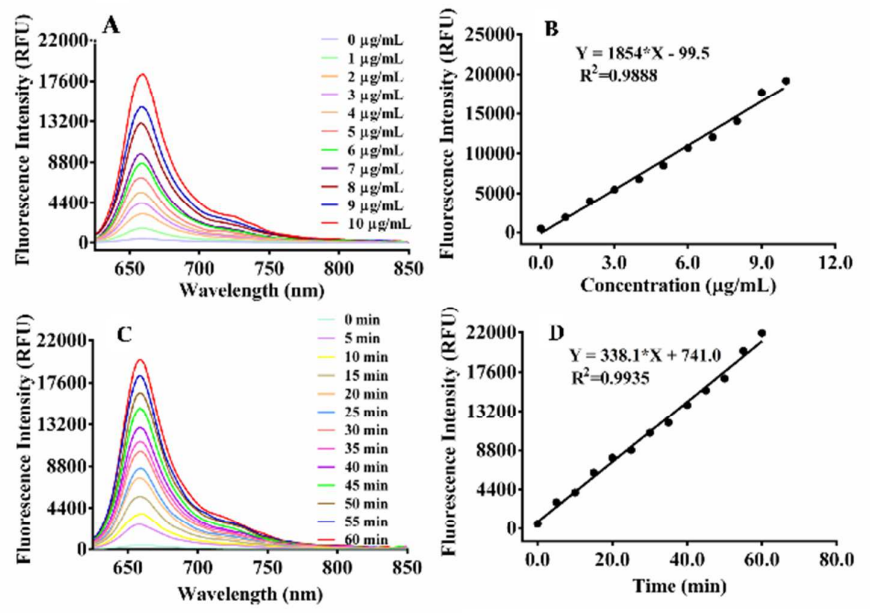

Figure S12. Fluorescence spectra and linear relationship of GLU concentration and reaction time. (A, B) Fluorescence spectra and linear relationship of **DDAO-glu** (10 μM) after increasing concentrations of GLU (0 − 10 μg/mL); (C, D) Fluorescence spectra and linear relationship of **DDAO-glu** (10μM) following with reaction time (0 − 60 min) at 37 °C. Spectra were acquired in PBS buffer (pH = 7.0) with the excitation at 600 nm.

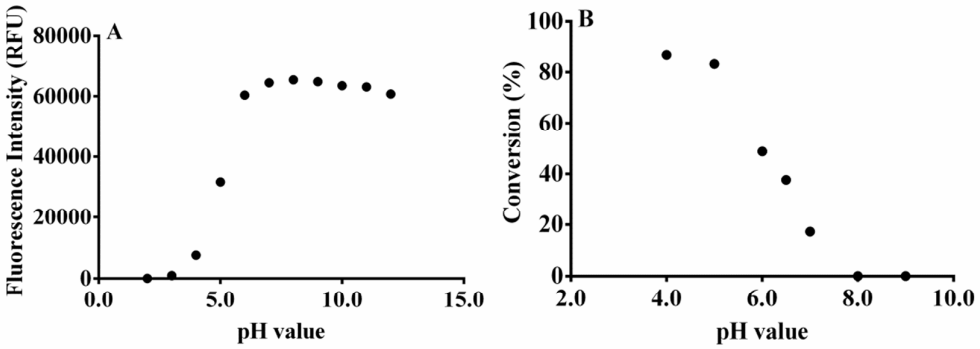

Figure S13. (A) The optimal pH values for fluorescent intensity of **DDAO** (1 μM) and (B) the effects of pH values on the activity of GLU.

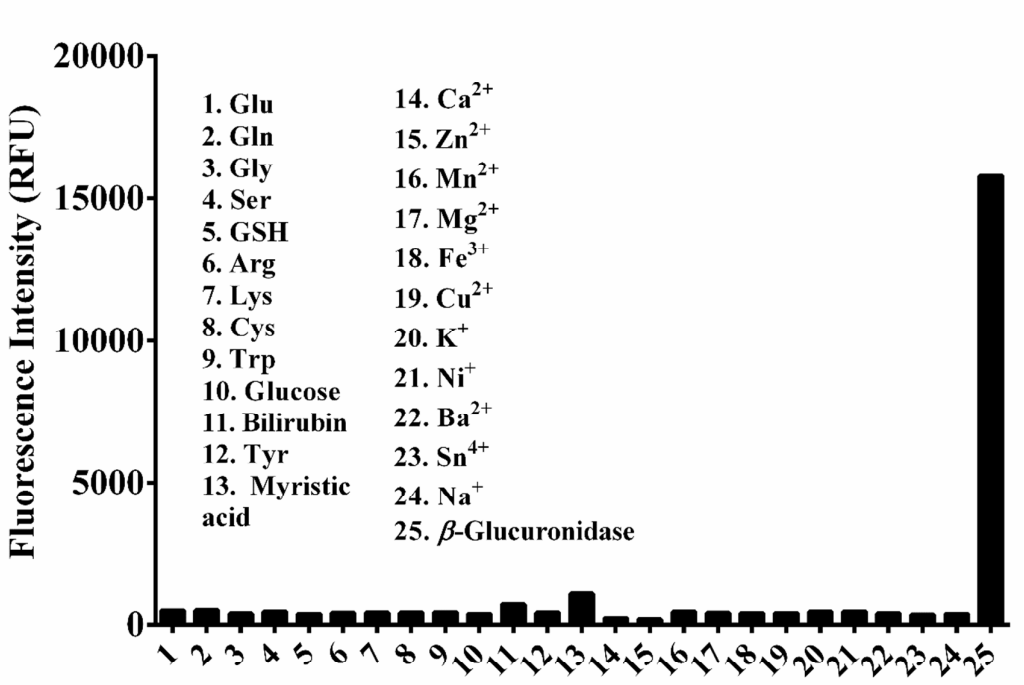

Figure S14. The influence of different endogenous and exogenous substances on the fluorescence intensities of **DDAO-glu** (10 μM) in Buffer/acetonitrile = 2: 1 system.

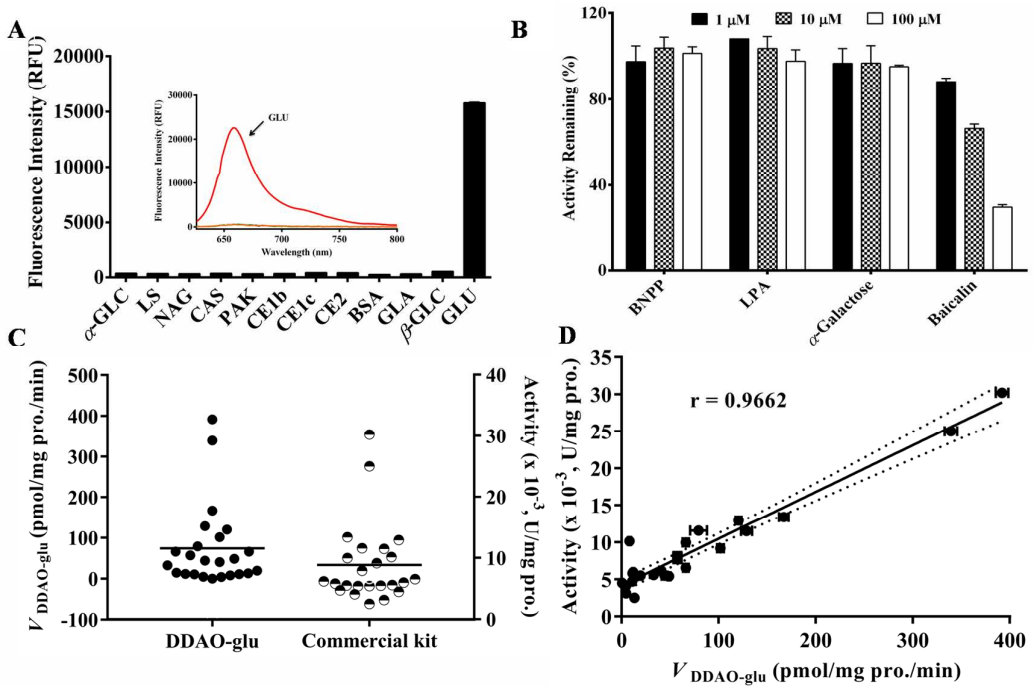

Figure S15. (A) Fluorescence responses of **DDAO-glu** (10 μM) towards various species of biological enzymes with the concentration of 10 μg/mL at 37 °C for 30 min. (B) Chemical inhibitions of **DDAO-glu** hydrolyzation by BNPP, LPA, *α*-Galactose and Baicalin in GLU incubation systems. (C) The activity levels of GLU detected by using **DDAO-glu** and Commercial kit in feces of 24 volunteers. (D) Correlation analysis between the hydrolytic rates of **DDAO-glu** and expression levels of GLU determined by Commercial kit in a panel of individual feces. (λ_{ex} 600 nm, λ_{em} 660 nm).

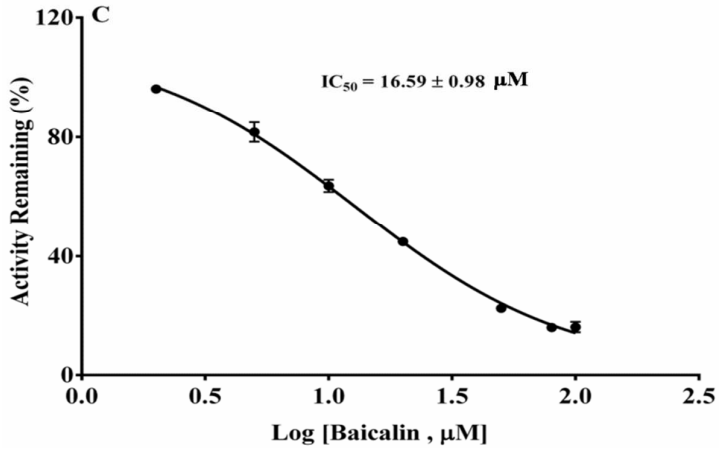

Figure S16. Dose-dependent inhibition behavior of baicalin towards the activity of GLU.

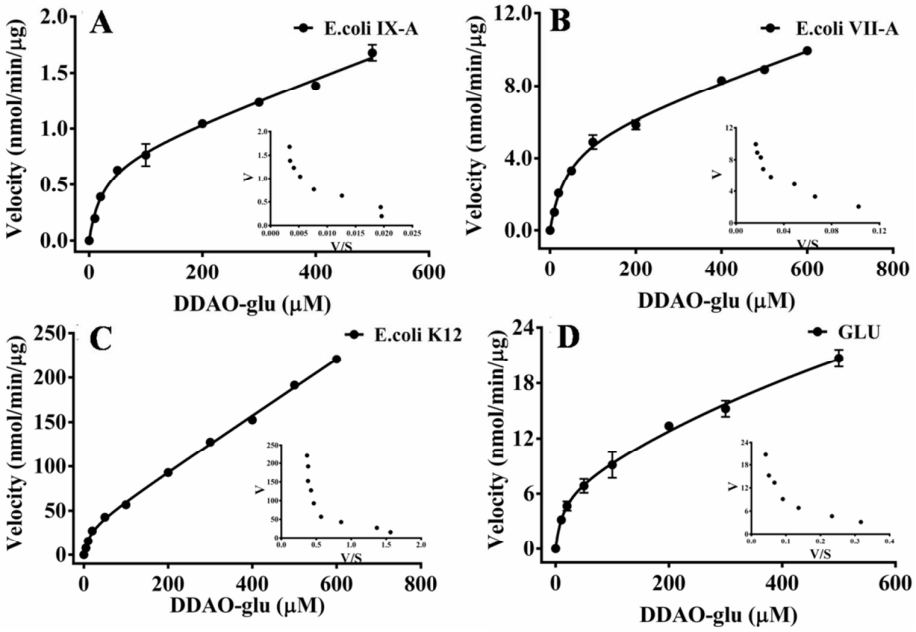

Figure S17. The kinetic analysis of **DDAO-glu** in different source of GLUs from (A) *E. coli* Type IX-A, (B) *E. coli* Type VII-A, (C) *E. coli K* 12, and (D) *E. coli* recombinant GLU , respectively.

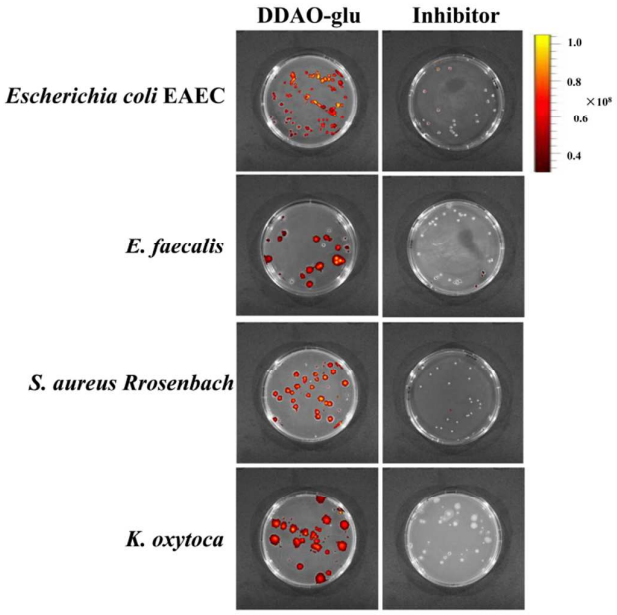

Figure S18. The fluorescence images of intestinal bacteria in plate medium using **DDAO-glu** to determine the endogenous GLU activities. Baicalin (200 μM) as the inhibitor of GLU was pretreated for bacteria before **DDAO-glu** incubation. **A.** *Escherichia coli* EAEC; **B**. *E. faecalis*; **C.** *S. aureus Rrosenbach*; **D.** *K. oxytoca*.

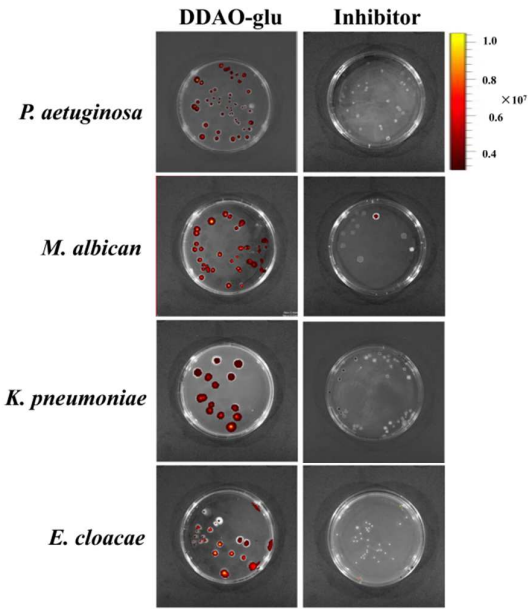

Figure S19. The fluorescence images of intestinal bacteria in plate medium using **DDAO-glu** to determine the endogenous GLU activities. Baicalin (200 μM) as the inhibitor of GLU was pretreated for bacteria before **DDAO-glu** incubation. **A.** *P. aetuginosa*; **B**. *M. albican*; **C.** *K. pneumoniae*; and **D.** *E. cloacae*.

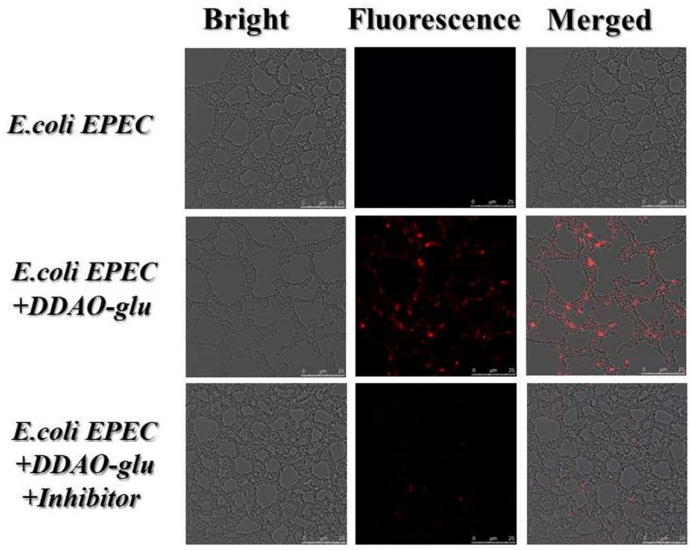

Figure S20. The fluorescence images of *E. coli* EPEC in liquid medium using **DDAO-glu** with or without GLU inhibitor baicalin to determine intercellular GLU activity. Baicalin (200 μM) as the inhibitor of GLU was pretreated for bacteria before **DDAO-glu** incubation.

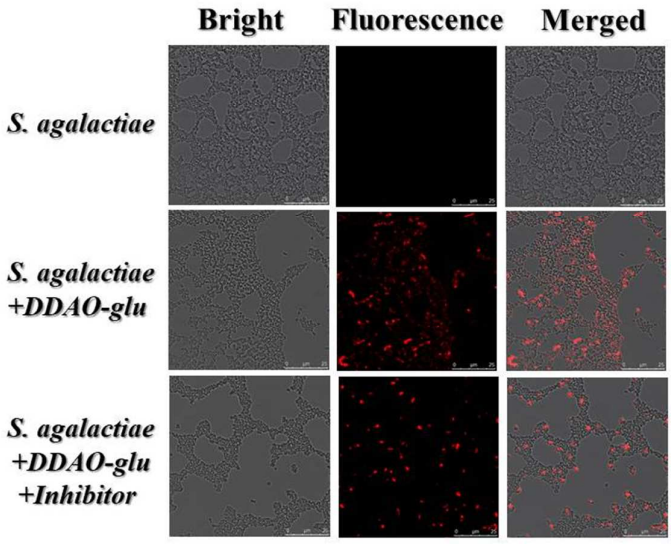

Figure S21. The fluorescence images of *S.agalactia* in liquid medium using **DDAO-glu** with or without GLU inhibitor baicalin to determine intercellular GLU activity. Baicalin (200 μM) as the inhibitor of GLU was pretreated for bacteria before **DDAO-glu** incubation.

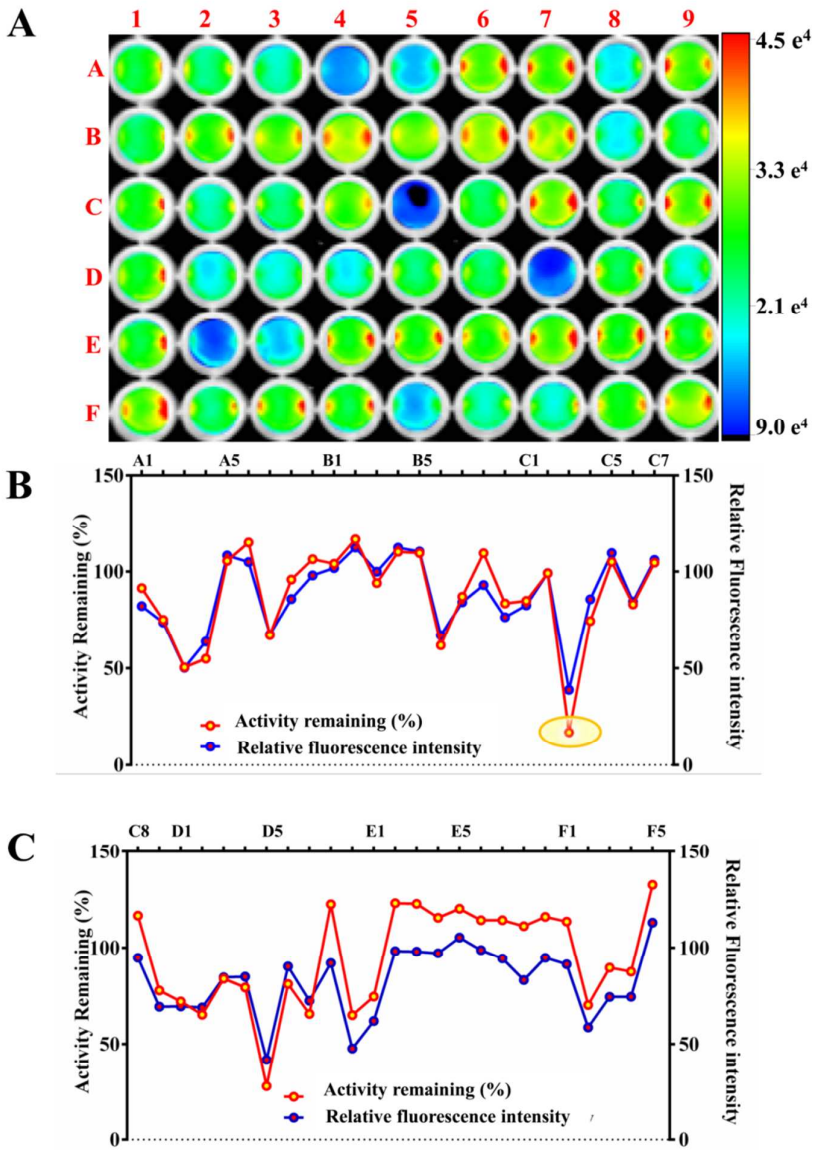

Figure S22. The inhibitory effects of 50 herbal medicines toward GLU. (A) Fluorescence images response to the inhibition effects of 50 medicinal herbs against GLU incubated with **DDAO-glu** (10 μM) in 96-well plates (λ_{ex} 630 nm, λ_{em} 665−735 nm). (B, C) Their inhibitory effects against GLU measured using **DDAO-glu** by microplate reader (blue, λ_{ex} 600 nm, λ_{em} 662 nm), and the remaining GLU activity (red) based on the relative fluorescence intensity of fluorescence images in each well of 96-well plate.

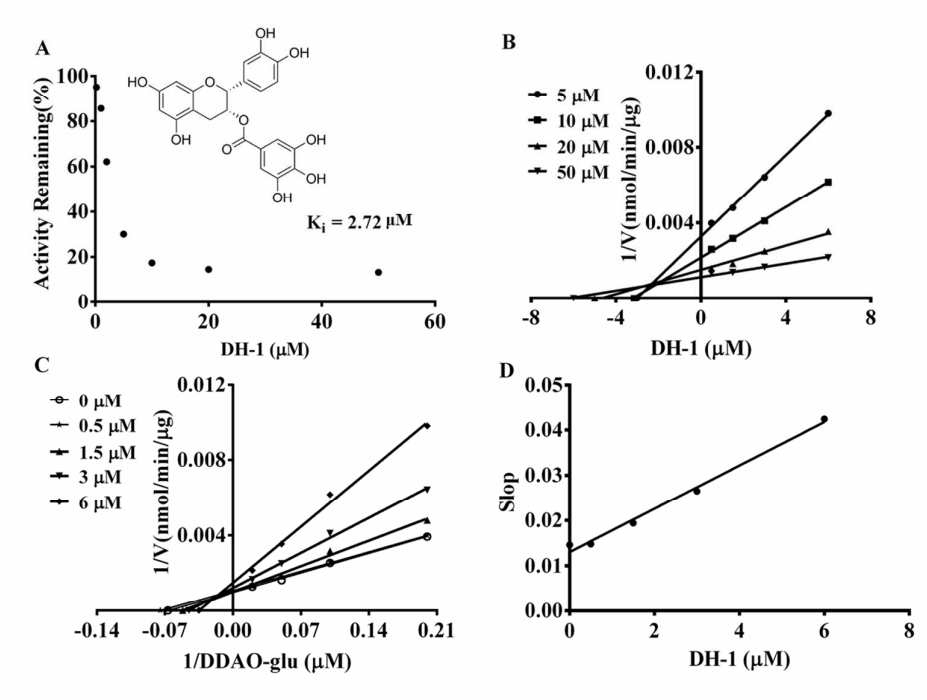

Figure S23. Dose-dependent inhibition behavior of **DH-1** towards the activity of GLU.

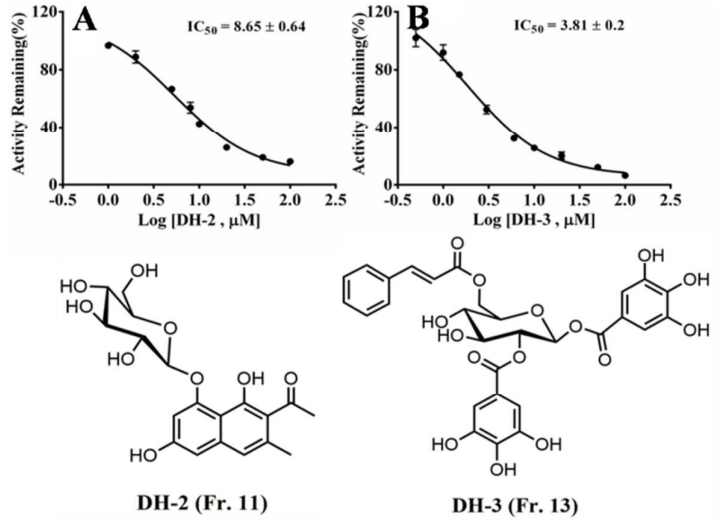

Figure S24. Dose-dependent inhibition behavior of **DH-2** and **DH-3** towards the activity of GLU.

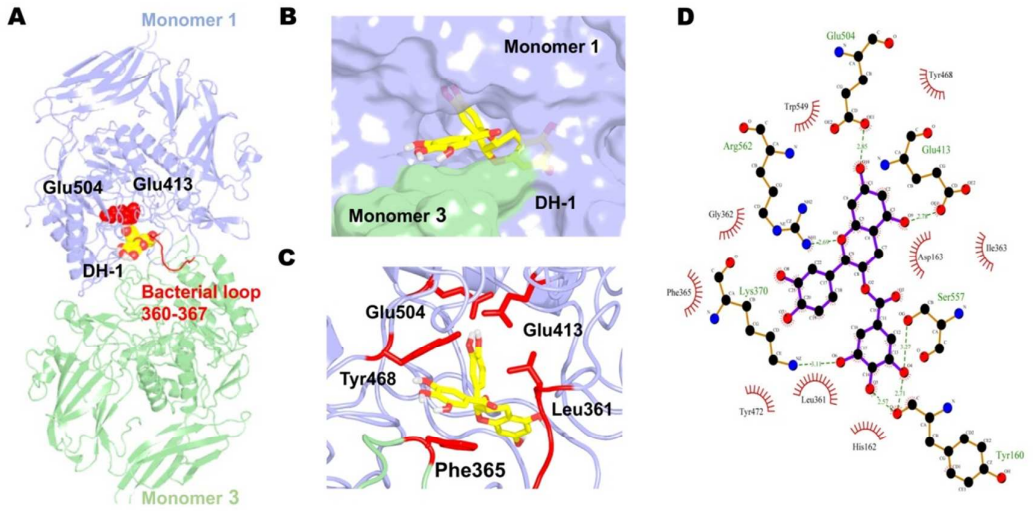

Figure S25. Computer simulation study of **DH-1** with bacterial *β*-Glucuronidase (GLU). (A) **ECG** was bound into the active site of eβG (PDB code: 3LPF) after molecular docking followed by 5ns MD simulation. Monomer 1 was depicted in blue cartoon and monomer 3 was depicted in green cartoon. Two catalytic residues Glu413 and Glu504 were displayed in red spheres. **ECG** was displayed in yellow and red CPK model. The unique bacterial loop was highlighted in red color (360 - 367); (B) The snug-fit-in model of **DH-1** complexed within the active site of eβG. **ECG** was displayed in stick model; (C) The predicted binding mode of **ECG** in the active site of eβG after MD simulation. Residues making critical contacts with **ECG** in the active site were highlighted in red sticks; (D) Representation of interactions of **ECG** in the active site of eβG prepared by Ligplot program.

Computer simulation study of DH-1 with bacterial *β*-Glucuronidase (GLU). Furthermore, we wanted to dissect the binding mechanism of **DH-1** complexed with GLU (PDB code: 3LPF) using molecular docking coupled with molecular dynamics (MD) simulation and MM/PBSA free energy calculation. Our MD results revealed that **DH-1** is bound deeply in the active site of GLU which is composed by two neighboring monomers (monomer-1 and monomer 3 of the GLU homotetramer structure. We observed that the para-hydroxyl group of 3,4-diphenol moiety on **DH-1** molecule enables three putative hydrogen bonding with the catalytic residues Glu413 and Glu504 as well as Tyr468 (with separation distances: 1.7 Å, 4.1 Å and 4.2 Å, respectively). Moreover, the ester oxygen atom on **DH-1** can form another putative hydrogen bonding with Leu361 (with a separation distance: 2.6 Å) located on the unique bacterial loop of GLU (res 360-367). In particular, the phenyl ring of the

tri-phenol moiety on **DH-1** can make putative π-π stacking with Phe365 in monomer 3 of GLU. Additionally, **DH-1** also maintains possible hydrophobic interactions with a few surrounding residues including Tyr468, Tyr549, Tyr472, His162 and Asp163 in the active site. Importantly, three residues in the bacterial loop also make hydrophobic contacts with **DH-1** including Leu361, Gly362 and Ile363. In line with the in vitro binding results, our MM/PBSA calculation shows that **DH-1** binds strongly with GLU with binding free energy of -200.635 kJ/mol. Collectively, our results show that **DH-1** binds to the active site and interacts with both monomer-1 and monomer 3 as well as the bacterial loop of GLU, indicating the strong inhibitory ability of **DH-1** against GLU from the perspective of computer simulation.

Table S1. Kinetic parameters and CL_{int} values of **DDAO-glu** in different source GLU from *E. coli*, *E. coli K* 12, *E. coli* Type IX-A and *E. coli* Type VII-A.

Enzymes	V_{m1} (nmol/min/μg)	V_{m2} (nmol/min/μg)	K_{m1} (μM)	K_{m2} (μM)	CL_{int1} (μL/min/μg)	CL_{int2} (μL/min/μg)
GLU (*E.coli*)	6.39 ± 1.52	57.0 ± 32.4	13.1 ± 6.57	1480 ± 1276	488	38.5
GLU (*E.coli*-IX-A)	0.734 ± 0.084	--	23.6 ± 6.95	--	31.2	--
GLU (*E.coli*-VII-A)	5.34 ± 0.540	--	39.7 ± 8.92	--	134	--
GLU (*E.coli*-K12)	31.7 ± 6.79	--	13.9 ± 6.67	--	2287	--

Table S2. Pharmacokinetic parameters of diclofenac after oral administration of diclofenac (10 mg/kg) with or without **ECG** (50 mg/kg) in rats. (mean ± S.E., n = 3)

Parameter	Unit	Diclofenac only	Diclofenac + ECG
T_{max1}	min	15.0 ± 0.0	15.0 ± 0.0
C_{max1}	μg/mL	3.89 ± 0.63	3.39 ± 0.40
T_{max2}	min	200 ± 11	300 ± 40 [a]
C_{max2}	μg/mL	1.87 ± 0.31	0.57 ± 0.061 [a]
$AUC_{(0\text{-}600)}$	μg/mL·min	478 ± 35	364 ± 45 [a]

[a] $p < 0.05$ vs Diclofenac only group.